expressed as ‰ (parts per thousand) deviation from the Canyon Diablo Troilite (CDT) standard and given by $10^3[(^{34}S/^{32}S)_{sam} - (^{34}S/^{32}S)_{CDT}]/(^{34}S/^{32}S)_{CDT}$.
7. J. M. Hayes, in *Earth's Earliest Biosphere, Its Origin and Evolution*, J. W. Schopf, Ed. (Princeton Univ. Press, Princeton, NJ, 1983), pp. 291–301; D. E. Canfield, *Nature* **396**, 450 (1998).
8. I. R. Kaplan and S. C. Rittenberg, *J. Gen. Microbiol.* **34**, 195 (1964); L. A. Chambers, P. A. Trudinger, J. W. Smith, M. S. Burns, *Can. J. Microbiol.* **21**, 1602 (1975).
9. H. Ohmoto and R. P. Felder, *Nature* **328**, 244 (1987); T. Kakegawa, H. Kawai, H. Ohmoto, *Geochim. Cosmochim. Acta* **62**, 3205 (1998).
10. J. B. Corliss *et al.*, *Science* **203**, 1073 (1979).
11. A. N. Roychoudhury, E. Viollier, P. Van Cappellen, *Appl. Geochem.* **13**, 269 (1998).
12. At 88°C, a large decrease in fractionation was observed with both limiting and nonlimiting substrate (Fig. 1A). This decrease was accompanied by a decrease in sulfate reduction rate (Fig. 1B), and we speculate that this high temperature approached the upper limit for growth by the sulfate-reducing population. Reduced fractionations are sometimes observed when organisms metabolize considerably outside of their optimal growth range (*8*), perhaps as a result of physiological stress on the organism.
13. The actual isotopic composition of Guaymas Basin sedimentary sulfides has yet to be reported, but a substantial mantle-derived hydrothermal source of sulfide could overprint biological fractionations from sulfate reduction [J. M. Peter and W. C. Shanks III, *Geochim. Cosmochim. Acta* **56**, 1025 (1992)].
14. On the basis of the temperature of maximum growth rate, organisms may be broadly classified into four major groups. Psychrophiles are organisms with growth optima below 20°C, and some may grow below the freezing point of water [R. M. Atlas and R. Bartha, *Microbial Ecology: Fundamentals and Applications* (Addison Wesley Longman, Menlo Park, CA, 1998), pp. 281–331]. Mesophiles have growth optima in the range of 20° to 45°C, thermophiles have their growth optima between 45° and 75°C, and hyperthermophiles have growth optima from 80° to 115°C (thus far, higher temperatures for metabolism are not known). For all organisms, growth rates are reduced at temperatures on either side of the optimal growth temperature. The highest specific rates of metabolism are generally found above the growth optima and, in some cases, even at temperatures above those where growth occurs (*30*). Continued metabolism at high rates above the maximum temperature for growth will result in mortality of the population. For sulfate-reducing bacteria metabolizing below the temperature of maximum specific rate, a 10°C increase in temperature causes an increase in rate of, typically, two to four times [J. T. Westrich and R. A. Berner, *Geomicrobiol. J.* **6**, 99 (1988)]. This rate of increase is known as the Q_{10}.
15. Factors other than specific rate of sulfate reduction can also influence isotope fractionation, including electron donor [H_2 produces reduced fractionations compared with organic substrates (*8*)] and physiological state of the organism (*12*). Furthermore, interspecies differences in isotope fractionation are possible, but as yet poorly explored.
16. The isotopic composition of sulfide in a closed system will match the isotopic composition of the original sulfate after sulfate depletion, regardless of the fractionation.
17. J. J. Middelburg, K. Soetaert, P. M. J. Herman, *Deep Sea Res. I* **44**, 327 (1997).
18. Our model assumes two types of organic carbon depositing to the sediment surface at equal concentrations and decomposing by sulfate reduction with first-order kinetics: $dC_i/dt = -k_iC_i$. In this expression, C_i represents the concentration of organic carbon of one type, t is time, and k_i is the intrinsic rate constant defining the reactivity of the organic carbon. We assume that the reactivity (k_i) of each of the two organic carbon fractions varies by two orders of magnitude, consistent with sediment observations [C. Rabouille, J.-F. Gaillard, J.-C. Relexans, P. Tréguer, M.-A Vincendeau, *Limnol. Oceanogr.* **43**, 420 (1998)]. We changed rates of sulfate reduction by changing the k_i values and solved the model analytically ("Modified Berner" model of B. P. Boudreau and J. T. Westrich [*Geochim. Cosmochim Acta* **48**, 2503 (1984)]].
19. Considerably higher fluxes of organic carbon to early Archean sediments would have required higher ocean nutrient concentrations and more active nutrient cycling, leading to much higher rates of photosynthetic primary production. We are unaware of any data supporting such high rates of carbon production and remineralization in the early Archean.
20. K. S. Habicht and D. E. Canfield, *Nature* **382**, 342 (1996).
21. ———, *Geochim. Cosmochim. Acta* **61**, 5351 (1997). High fractionations (25 to 30‰) are also preserved in rapidly depositing continental margin sediments experiencing relatively rapid rates of sulfate reduction (up to 0.5 mol liter^{-1} year^{-1}) and with sulfate depletion at the shallow depth of 10 to 20 cm [J. P. Chanton, C. S. Martens, M. B. Goldhaber, *Geochim. Cosmochim. Acta* **51**, 1201 (1987); J. Val Klump and C. S. Martens, *Geochim. Cosmochim. Acta* **51**, 1161 (1987)].
22. A sulfate level of around 2.0 mM has been suggested for 3.2-Ga seawater from the analysis of fluid inclusions within quartz veinlets and vugs dispersed within ironstone pods believed to be precipitated in a sea floor hydrothermal vent setting [C. E. J. de Ronde, D. M. deR. Channer, K. Faure, C. J. Bray, E. T. C. Spooner, *Geochim Cosmochim. Acta* **61**, 4025 (1997)]. Although this is a low concentration compared with modern seawater, our results support even lower Archean seawater sulfate concentrations.
23. A. G. Harrison and H. G. Thode, *Trans. Faraday Soc.* **53**, 84 (1958).
24. Phylogenies constructed from sequence comparisons of the 16*S* ribosomal RNA molecule show thermophilic sulfate-reducing bacteria of the genus *Thermodesulfobacterium* branching more deeply within the Bacterial domain than the lineage housing Cyanobacteria [E. Stackebrandt, D. A. Stahl, R. Devereux, in *Sulfate-Reducing Bacteria*, L. L. Barton, Ed. (Plenum, New York, 1995), pp. 49–87; N. R. Pace, *Science* **276**, 734 (1997)]. This observation supports an early evolution of sulfate-reducing bacteria, predating the evolution of oxygen-producing Cyanobacteria.
25. E. M. Cameron and K. Hattori, *Chem. Geol.* **65**, 341 (1987).
26. A. M. Goodwin, J. Monster, H. G. Thode, *Econ. Geol.* **71**, 870 (1976); H. G. Thode and A. M. Goodwin, *Precambrian Res.* **20**, 337 (1983).
27. A. H. Knoll and D. E. Canfield, in *Isotope Paleobiology and Paleoecology*, R. N. Norris and R. M. Corfield, Eds. (Paleontological Society, Pittsburgh, PA, 1998), pp. 212–243; D. E. Canfield and R. Raiswell, *Am. J. Sci.* **299**, 697 (1999); E. M. Cameron, *Nature* **296**, 145 (1982).
28. J. J. Brocks, G. A. Logan, R. Buick, R. E. Summons, *Science* **285**, 1033 (1999).
29. Supplemental data are available at www.sciencemag.org/feature/data/1048533.shl.
30. C. Knoblauch, B. B. Jørgensen, J. Harder, *Appl. Environ. Microbiol.* **65**, 4230 (1999).
31. M. E. Böttcher, S. M. Sievert, J. Kuever, *Arch. Microbiol.* **172**, 125 (1999).
32. We are indebted to the late H. Jannasch and A. Teske for arranging a wonderful cruise to the Guaymas Basin and to the *Alvin* and *Atlantis* crews for their expert technical support. We thank J. Nielsen, Y. Shen, R. Buick, and two anonymous reviewers for critical comments and L. Salling for help in the lab. Generous support was provided by the Danish National Research Foundation and the Madam Curie Training Program of the EU.

11 January 2000; accepted 21 March 2000

Heightened Odds of Large Earthquakes Near Istanbul: An Interaction-Based Probability Calculation

Tom Parsons,[1]* Shinji Toda,[2] Ross S. Stein,[1] Aykut Barka,[3] James H. Dieterich[1]

We calculate the probability of strong shaking in Istanbul, an urban center of 10 million people, from the description of earthquakes on the North Anatolian fault system in the Marmara Sea during the past 500 years and test the resulting catalog against the frequency of damage in Istanbul during the preceding millennium. Departing from current practice, we include the time-dependent effect of stress transferred by the 1999 moment magnitude M = 7.4 Izmit earthquake to faults nearer to Istanbul. We find a 62 ± 15% probability (one standard deviation) of strong shaking during the next 30 years and 32 ± 12% during the next decade.

The 17 August 1999 **M** = 7.4 Izmit and 12 November 1999 **M** = 7.1 Düzce earthquakes killed 18,000 people, destroyed 15,400 buildings, and caused $10 billion to $25 billion in damage. But the Izmit event is only the most recent in a largely westward progression of seven large earthquakes along the North Anatolian fault since 1939. Just northwest of the region strongly shaken in 1999 lies Istanbul, a rapidly growing city which has been heavily damaged by earthquakes 12 times during the past 15 centuries. Here, we calculate the probability of future earthquake shaking in Istanbul, using new concepts of earthquake interaction, in which the long-term renewal of stress on faults is perturbed by transfer of stress from nearby events.

Stress triggering has been invoked to explain the 60-year sequence of earthquakes rupturing

[1]U.S. Geological Survey, Menlo Park, CA 94025, USA. [2]Earthquake Research Institute, University of Tokyo, Tokyo, 113-0032 Japan. [3]Istanbul Technical University, Istanbul, 80626 Turkey.

*To whom correspondence should be addressed. E-mail: tparsons@usgs.gov

toward Istanbul (*1–3*), in which all but one event promoted the next (*4*). Although an earthquake drops the average stress on the fault that slipped, it also changes the stress elsewhere. The seismicity rate has been observed to rise in regions of stress increase and fall where the off-fault stress decreases (*5, 6*). The **M** = 7.4 Izmit earthquake, as well as most background seismicity (*7*), occurred where the failure stress is calculated to have increased by 1 to 2 bars (0.1 to 0.2 MPa) because of **M** ≥ 6.5 earthquakes since 1939 (Fig. 1A) (*8*). The Izmit event, in turn, increased the stress beyond the east end of the rupture by 1 to 2 bars, where the **M** = 7.2 Düzce earthquake struck, and by 0.5 to 5.0 bars beyond the west end of the 17 August 1999 rupture, where a cluster of aftershocks occurred (Fig. 1B). The correspondence seen here between calculated stress changes and the occurrence of large and small earthquakes, also reported in (*9*), strengthens the rationale for incorporating stress transfer into a seismic hazard assessment.

A probabilistic hazard analysis is no better than the earthquake catalog on which it is based. Global observations support an earthquake renewal process in which the probability of a future event grows as the time from the previous event increases (*10*). To calculate such a renewal probability, ideally, one wants an earthquake catalog containing several large events on each fault to deduce earthquake magnitudes, the mean interevent time of similar events, and the elapsed time since the last shock on each fault (*11*). Although such catalogs are rarely, if ever, available, Ambraseys and Finkel compiled a wealth of earthquake damage descriptions for events since A.D. 1500 in the Marmara Sea region (*12–15*). We assigned modified Mercalli intensities (MMI) to 200 damage descriptions (*16*), and used the method of Bakun and Wentworth (*17*) to infer **M** and epicentral location from MMI through an empirical attenuation relation (*18*). We calibrated the relation against Marmara Sea events that have both intensity and instrumental data (*19*). Uncertainties in earthquake location were explicitly calculated from MMI inconsistencies and inadequacies.

Our catalog thus consists of nine **M** ≥ 7 earthquakes in the Marmara Sea region since 1500. For the six events that occurred before instrumental recording began in 1900, we selected the minimum magnitude falling within the 95% confidence bounds at locations associated with faults of sufficient length (*20*) to generate the event (Fig. 2). We estimated rupture lengths and the mean slip from empirical relations on **M** for continental strike-slip faults (*21*). The locations and geometry of faults in the Marmara Sea are under debate; we follow (*20*), which is based on seismic reflection profiles (Fig. 2), and find four faults capable of producing strong shaking in Istanbul: the Yalova, Izmit, Prince's Islands, and central Marmara faults. Our catalog suggests two earthquakes on the Izmit fault (occurring in 1719 and 1999), yielding an interevent time of ~280 years, and three on the Yalova fault (1509, 1719, 1894), permitting an estimate of ~190 years (*22*). We infer one earthquake (May 1766) on the Prince's Islands fault and one (1509) on the central Marmara fault (Fig. 2). For these, we gauge interevent times by dividing the seismic slip estimated from the catalog by the global positioning system (GPS)–derived slip rate (*23, 24*), yielding interevent times of ~210 years for the Prince's Islands fault and ~540 years for the central Marmara fault. Thus, at least two of the four faults are likely late in their earthquake cycles.

One way to validate the catalog magnitudes, locations, and segment interevent times is to compare the relative abundance of small to large shocks through the *b*-value; another is to see if the seismic strain release from the catalog is consistent with the measured strain accumulation from GPS. The frequency-magnitude relation for our catalog yields b = 1.1 by maximum likelihood (*25*), close to the

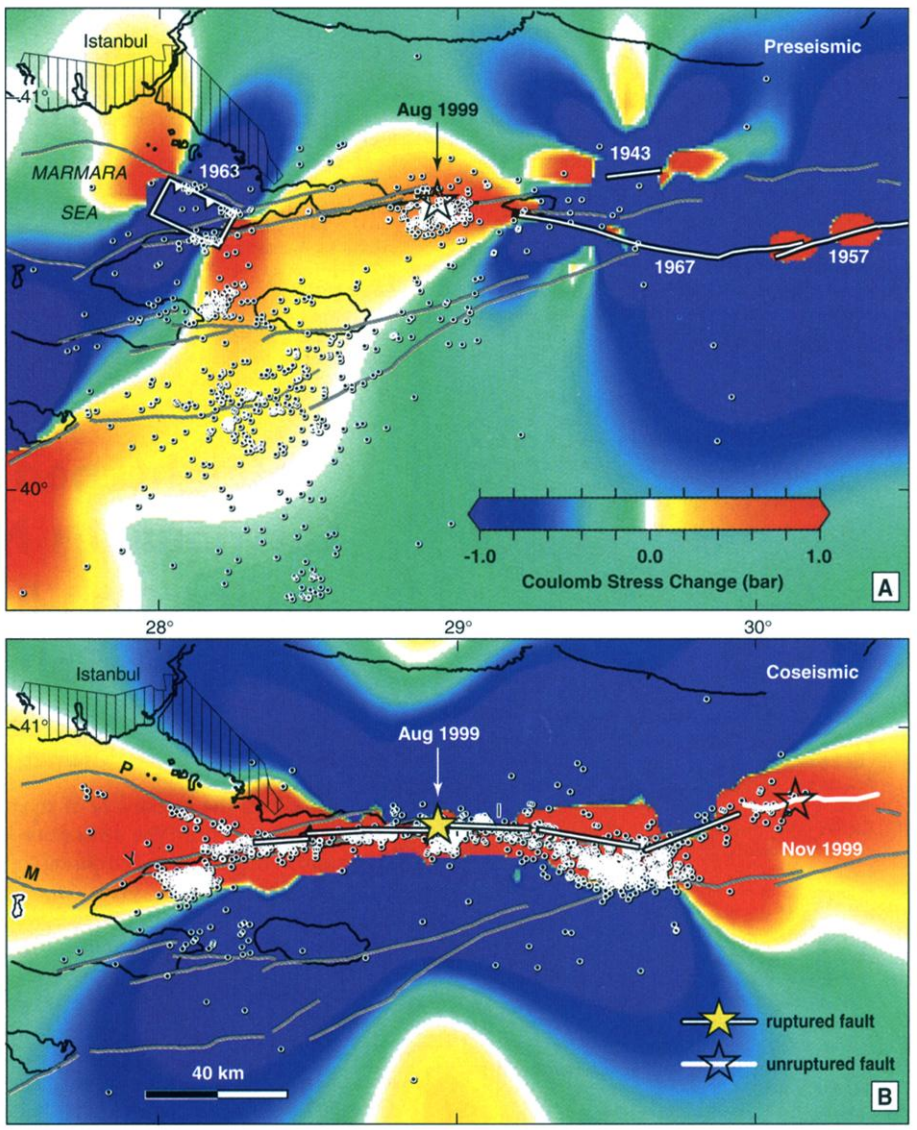

Fig. 1. (**A**) Stress change caused by earthquakes since 1900. Shown are the maximum Coulomb stress changes between 0 and 20 km depth on optimally oriented vertical strike-slip faults (*44*). The assumed friction coefficient is 0.2, as has been found for strike-slip faults with large cumulative slip (*45, 46*). A 100-bar deviatoric tectonic stress with compression oriented N55°W (*47*) is used, under which optimally oriented right-lateral faults strike E-W except along the rupture surface. The 1993 to July 1999 seismicity recorded since installation of IZINET (*7*) has uniform coverage over the region shown. Calculated stress increases are associated with heightened seismicity rates and with the future epicenter of the 17 August 1999 Izmit earthquake (indicated by star); sites of decreased stress exhibit low seismicity. (**B**) Izmit aftershocks are associated with stress increases caused by the main rupture [first 12 days from IZINET (*7*)], such as the Yalova cluster southeast of "Y," and the occurrence of the 12 November 1999 Düzce earthquake. Faults: Y, Yalova; P, Prince's Islands; M, Marmara; I, Izmit.

global average (*26*). Over a sufficiently long time period, the moment release by earthquakes must balance the moment accumulation by elastic strain if aseismic creep is negligible. We compared the seismic slip rate represented by the catalog (23.5 ± 8 mm/year) to the observed slip rate measured by GPS across the North Anatolian fault system in the Marmara region (22 ± 3 mm/year) (quoted uncertainties are one standard deviation here and elsewhere) (Fig. 3) (*27*). For $b \sim 1$, most of the moment is conferred by the largest shocks, so the consistency between GPS and catalog strain means that the size and location of the three **M** ~ 7.6 events, as well as the number of smaller earthquakes, are plausible.

Perhaps the strongest test of the 500-year catalog can be made by calculating the combined Poisson, or time-independent, probability predicted from the interevent times for the three faults we regard as capable of producing MMI ≳ VIII shaking in Istanbul. This is the probability averaged over several earthquake cycles on each fault and yields 29 ± 15% in 30 years. This can be compared to the Poisson probability calculated directly from the longer record of MMI ≳ VIII shaking in Istanbul during the preceding ~1000 years (A.D. 447 to 1508). The older record gives the long-term frequency of shaking used in a Poisson calculation without knowledge of the earthquake locations. At least eight earthquakes (*28*) caused severe damage in Istanbul from A.D. 447 to 1508 (*12–14*), translating into a 20 ± 10% 30-year probability, roughly comparable to that derived from our catalog. Thus, the fault interevent times estimated from the 500-year catalog are consistent with the independent record of shaking in Istanbul during the preceding millennium.

We combined earthquake renewal and stress transfer into the probability calculation on the basis that faults with increased stress will fail sooner than unperturbed faults. Because two of the three faults within 50 km of Istanbul are interpreted to be late in their earthquake cycles, the renewal probability is higher than the Poisson probability. Additionally, the permanent probability gain caused by stress increase is amplified by a transient gain that decays with time. The transient gain is an effect of rate- and state-dependent friction (*29–31*), which describes behavior seen in laboratory experiments and in natural seis-

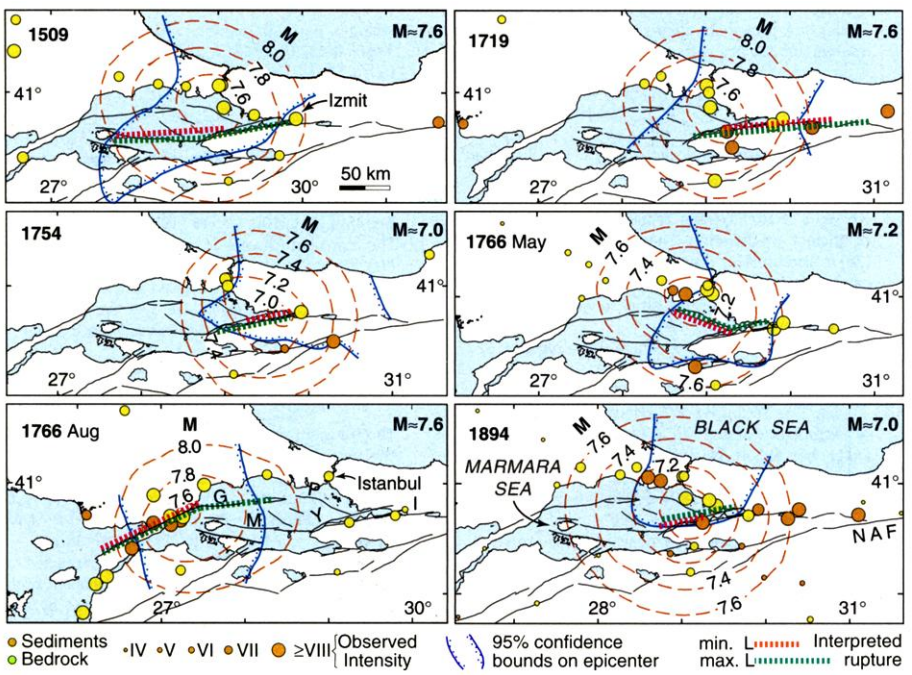

Fig. 2. Large historical earthquakes since 1500. Intensities (dots) were assigned from damage descriptions compiled by (*12–15*). Red dashed contours give the moment magnitude **M** needed to satisfy the observations for a given location (*17*), because the farther the epicenter is from the observations, the larger the **M** required to satisfy them. The confidence on location is governed by the relative intensities; magnitude is a function of absolute intensities. We assigned earthquakes to faults by minimizing **M** within the 95% confidence region (*18, 19*). Faults labeled in lower panels: I, Izmit; Y, Yalova; P, Prince's Islands; M, Marmara; G, Ganos; NAF, North Anatolia fault.

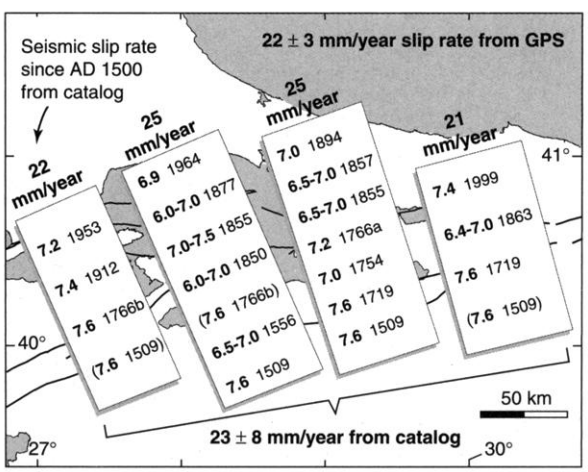

Fig. 3. Seismic slip from the 500-year-long catalog of Fig. 2 is summed in four transects across the North Anatolia fault system in the Marmara Sea. All known or estimated **M** ≳ 7 sources are included (*27*). The mean seismic strain release rate balances the strain accumulation rate observed from GPS geodesy (*24*). Whether earthquakes in parentheses extend to a given transect is uncertain. "1766a" is May; "1766b" is August.

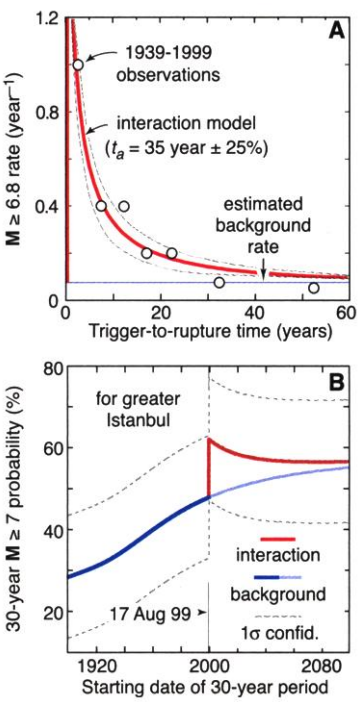

Fig. 4. (**A**) Observed and modeled transient response to stress transfer. The 13 **M** ≥ 6.8 North Anatolian earthquakes for which the stress at the future epicenter was increased by ≥0.5 bars are plotted as a function of time. The earthquake rate decays as t^{-1} in a manner identical to aftershocks, as predicted by (*29–32*). (**B**) Calculated probability of a **M** ≥ 7 earthquake (equivalent to MMI ≳ VIII shaking in greater Istanbul) as a function of time. The probability on each of three faults is summed (*43*). The large but decaying probability increase is caused by the 17 August 1999 Izmit earthquake. "Background" tracks the probability from earthquake renewal; "interaction" includes renewal and stress transfer. Light blue curve gives the probability had the Izmit earthquake not occurred.

Table 1. Earthquake probabilities for faults within 50 km of Istanbul beginning May 2000. "Combined" is the probability for the three faults (*43*). Quoted uncertainties are one standard deviation. "Background" refers to renewal; "interaction" includes renewal and interaction by stress transfer.

Fault	30-year (%)		10-year (%)		1-year (%)	
	Interaction	Background	Interaction	Background	Interaction	Background
Yalova	33 ± 21	22 ± 18	14 ± 11	7 ± 7	1.7 ± 1.7	0.8 ± 0.8
Prince's Islands	35 ± 15	26 ± 12	16 ± 9	10 ± 6	2.1 ± 1.6	1.1 ± 0.7
Marmara	13 ± 9	11 ± 8	5 ± 5	4 ± 4	0.6 ± 0.7	0.5 ± 1.0
Combined	62 ± 15	49 ± 15	32 ± 12	20 ± 9	4.4 ± 2.4	2.3 ± 1.5

mic phenomena, such as earthquake sequences, clustering, and the occurrence of aftershocks. We estimated the duration of the transient decay directly from the times between triggering and rupturing earthquakes on the North Anatolian fault (Fig. 4A). Because parameter assignments used in the calculation are approximate, we performed a Monte Carlo simulation to explore the uncertainties (*32*). The resulting probability functions (Fig. 4B) exhibit a gradual rise as the mean time since the last shock on each fault grows, then a sharp jump in August 1999 followed by a decay. We find a 62 ± 15% probability of strong shaking [MMI ≥ VIII; equivalent to a peak ground acceleration of 0.34 to 0.65*g* (*33*)] in greater Istanbul over the next 30 years (May 2000 to May 2030), 50 ± 13% over the next 22 years, and 32 ± 12% over the next 10 years (Table 1). Inclusion of renewal doubles the time-averaged probability; interaction further increases the probability by a factor of 1.3.

The 12 earthquakes that damaged Istanbul during the past 1500 years attest to a significant hazard and form the basis for a 30-year Poisson, or time-averaged, probability of 15 to 25%. Because the major faults near Istanbul are likely late in their earthquake cycles (with no major shocks since 1894), the renewal probability climbs to 49 ± 15%. We calculate that stress changes altered the rate of seismicity after the 1999 Izmit earthquake, promoting the **M** = 7.2 Düzce shock and the Yalova cluster. Because the 1999 Izmit shock is calculated to have similarly increased stress on faults beneath the Marmara Sea, the interaction-based probability we advocate climbs still higher, to 62 ± 15%.

References and Notes

1. I. Ketin, *Bull. Min. Res. Explor. Inst. Turkey* **72**, 1 (1969).
2. A. A. Barka, *Bull. Seismol. Soc. Am.* **86**, 1238 (1996).
3. M. N. Toksoz, A. F. Shakal, A. J. Michael, *Pure Appl. Geophys.* **117**, 1258 (1979).
4. R. S. Stein, A. A. Barka, J. H. Dieterich, *Geophys. J. Int.* **128**, 594 (1997).
5. R. A. Harris, *J. Geophys. Res.* **103**, 24347 (1998).
6. R. S. Stein, *Nature* **402**, 605 (1999).
7. A. Ito *et al.*, *Eos* (*Fall Meet. Suppl.*) **80**, F662 (1999).
8. We calculate Coulomb failure stress [$\Delta CF \equiv \Delta|\bar{\tau}_f| + \mu'(\Delta\sigma_n)$, $\mu' = \mu(1 - B_k)$], where $\Delta\bar{\tau}_f$ is the change in shear stress on the receiver fault, μ is the coefficient of friction, $\Delta\sigma_n$ is the change in normal stress, and B_k is Skempton's coefficient. Stress values are found by elastic dislocation in a half space (*34*); viscoelastic effects are neglected. We used a slip model for the Izmit earthquake developed from InSAR (radar satellite interferometry) (*35*); slip models of other earthquakes are from (*4, 36*).
9. A. Hubert-Ferrari *et al.*, *Nature* **404**, 269 (2000).
10. Y. Ogata, *J. Geophys. Res.* **104**, 17995 (1999).
11. We use a probability density function $f(t)$ that describes how probability grows with time. Over a time interval, probability is found by
$$P(t \leq T \leq t + \Delta t) = \int_t^{t+\Delta t} f(t)dt$$
We use two probability distributions. The Brownian passage time function of Matthews (*37*) takes the form $f(t,\mu,\alpha) = (\mu/2\pi\alpha^2t^3)^{1/2}\exp[(t - \mu)^2/(2\pi\alpha^2t)]$, where μ is the average repeat time and α is the coefficient of variation. The lognormal distribution (*38*) is also used for time-dependent calculations. No catalog is adequate to estimate the coefficient of variation of the interevent time, so we use a conservative value of 0.5 (*10, 39*).
12. N. N. Ambraseys and C. F. Finkel, *Terra Nova* **3**, 527 (1991).
13. ———, *Terra Nova* **2**, 167 (1990).
14. ———, *The Seismicity of Turkey and Adjacent Areas: A Historical Review, 1500–1800* (Muhittin Salih EREN, Istanbul, Turkey, 1995).
15. C. F. Finkel and N. N. Ambraseys, *The Marmara Sea Earthquake of 10 July 1894 and its Effect on Historic Buildings, Anatolia Moderna Yeni Anadolu VII* (Bibliothèque de l'Institut Français d'Etudes Anatoliennes-Georges Dumézil, Paris, 1996), vol. 43.
16. Supplemental material is available at www.sciencemag.org/feature/data/1049447.shl.
17. W. H. Bakun and C. M. Wentworth, *Bull. Seismol. Soc. Am.* **87**, 1502 (1997).
18. The relation $\mathbf{M}_i = (\mathrm{MMI}_i + 3.29 + 0.0206d_i)/1.68$, where d_i is distance in kilometers between intensity observation and epicenter, was developed from 30 California shocks with both intensity and instrumental observations. The root mean square (rms) fit to this relation is calculated for trial locations on a grid with spaces of 5 km^2. Felt reports (MMI < IV) were excluded, and MMI > VIII observations were saturated to VIII because criteria for higher intensities involve observations other than building damage, and because for poorly constructed masonry, damage may be total at MMI = VIII.
19. We calibrated with the 1912 M_s = 7.4 Saros-Marmara [360 intensities (*40*)], 1963 M_s = 6.4 Yalova [11 intensities (*41*)], and 1999 **M** = 7.4 Izmit earthquakes (185 intensities). For the 1912 and 1999 events, we randomly selected 50 sets of 25 intensities (the mean number for the historical shocks) to calculate epicentral and magnitude errors. This yields intensity centers within ±50 km (at 95% confidence) of the instrumental epicenters and gives the correct **M** or M_s within ±0.3 magnitude units. Site corrections were not made, because we find no tendency for epicenters to be pulled toward sedimentary sites, and because improvement was only found in (*17*) when detailed site geology was available.
20. J. R. Parke *et al.*, *Terra Nova* **11**, 223 (1999).
21. D. L. Wells and K. J. Coppersmith, *Bull. Seismol. Soc. Am.* **84**, 974 (1994).
22. The most recent event for the Yalova segment is 1894.6; Izmit segment, 1999.7; Ganos fault, 1912.7; Prince's Islands fault, 1766.7; and central Marmara fault, 1509.8.
23. Working Group on California Earthquake Probabilities, *Bull. Seismol. Soc. Am.* **85**, 379 (1995).
24. C. Straub, H.-G. Kahle, C. Schindler, *J. Geophys. Res.* **102**, 27587 (1997).
25. K. Aki, *Bull. Earthquake Res. Inst.* **43**, 237 (1965).
26. S. G. Wesnousky, *Bull. Seismol. Soc. Am.* **89**, 1131 (1999).
27. Includes earthquakes in 1509, 1556, 1719, 1754, 1766, 1855, 1857, 1863, 1877, 1894, 1953, and 1964 from (*12–14, 36*).
28. Events occurring in A.D. 447, 478, 542, 557, 740, 869, 989, and 1323.
29. J. Dieterich, *J. Geophys. Res.* **99**, 2601 (1994).
30. J. H. Dieterich and B. Kilgore, *Proc. Natl. Acad. Sci. U.S.A.* **93**, 3787 (1996).
31. S. Toda, R. S. Stein, P. A. Reasenberg, J. H. Dieterich, *J. Geophys. Res.* **103**, 24543 (1998).
32. The transient change in expected earthquake rate $R(t)$ after a stress change, $R(t) = r/[\exp(-\Delta\tau/a\sigma) - 1]\exp(-t/t_a) + 1$, can be related to the probability of an earthquake of a given size over the time interval Δt through a nonstationary Poisson process as
$$P(t,\Delta t) = 1 - \exp\left[-\int_t^{t+\Delta t} R(t)dt\right]$$
The transient probability change is superimposed on the permanent change, which results from an advance or delay in the expected time until failure caused by the stress change. Integrating for is the expected number of earthquakes in the interval Δt, $N(t)$ yields $N(t) = r_p\{\Delta t + t_a\ln([1 + [\exp(-\Delta\tau/a\sigma) - 1]\exp(-t/t_a)]/\exp(-\Delta\tau/a\sigma))\}$, where r_p is the expected rate of earthquakes associated with the permanent probability change. This rate can be determined by again applying a stationary Poisson probability expression as $r_p = (-1/\Delta t)\ln(1 - P_c)$, where P_c is a conditional probability, which can be calculated using any distribution. In addition to the interevent time and elapsed time on each fault, this technique requires values for the stress change on each fault (we use the average calculated stress change resolved on each fault surface), the transient decay [shown in Fig. 4A from data in (*4*)], and a stressing rate on each fault derived from the fault geometry and the observed strain rate (0.1 bar/year) (*4*). We performed 1000 Monte Carlo trials to establish error bounds (*42*). The four parameters for the Monte Carlo simulations are drawn at random from a normal distribution with a shape factor of 0.25 about each estimate, except for the interevent time for which the shape factor is 0.5. Alternating Monte Carlo trials were run with a Brownian passage time and lognormal distribution.
33. D. J. Wald, V. Quitoriano, T. H. Heaton, H. Kanamori, *Earthquake Spectra* **15**, 557 (1999).
34. Y. Okada, *Bull. Seismol. Soc. Am.* **82**, 1018 (1992).
35. T. J. Wright, P. C. England, E. J. Fielding, M. Haynes, B. E. Parsons, *Eos* (*Fall Meet. Suppl.*) **80**, F671 (1999).
36. S. S. Nalbant, A. Hubert, G. C. P. King, *J. Geophys. Res.* **103**, 24469 (1998).
37. M. V. Matthews, *J. Geophys. Res.*, in press.
38. Working Group on California Earthquake Probabilities, *U.S. Geol. Surv. Circ. 1053* (1990).
39. ———, *U.S. Geol. Surv. Open File Rep. 99-517* (1999).
40. N. N. Ambraseys and C. F. Finkel, *Annales Geophysicae* **5B**, 701 (1987).
41. N. N. Ambraseys, *Earthquake Eng. Struct. Dyn.* **17** 1 (1988).
42. J. C. Savage, *Bull. Seismol. Soc. Am.* **81**, 862 (1991).

43. The combined probability expression $P = 1 - (1 - P_a)(1 - P_b)(1 - P_c)$ for faults a through c assumes independent sources of hazard, since we cannot include future interactions and, for all but the most recent earthquakes, we cannot include past interactions.
44. G. C. P. King, R. S. Stein, J. Lin, *Bull. Seismol. Soc. Am.* **84**, 935 (1994).
45. P. A. Reasenberg and R. W. Simpson, *Science* **255**, 1687 (1992).
46. T. Parsons, R. S. Stein, R. W. Simpson, P. A. Reasenberg, *J. Geophys. Res.* **104**, 20183 (1999).
47. C. Gürbüz *et al.*, *Tectonophysics* **316**, 1 (2000).
48. We thank N. Ambraseys, T. Wright, E. Fielding, A. Ito, J. Parke, and C. Finkel for sharing their insights and preliminary results with us, W. Bakun for his code and his review, and J. C. Savage, W. Thatcher, C. Straub, and S. Kriesch for incisive reviews. Support from *SwissRe* is gratefully acknowledged.

14 February 2000; accepted 27 March 2000

Extension of Cell Life-Span and Telomere Length in Animals Cloned from Senescent Somatic Cells

Robert P. Lanza,[1]* Jose B. Cibelli,[1] Catherine Blackwell,[1] Vincent J. Cristofalo,[2] Mary Kay Francis,[2] Gabriela M. Baerlocher,[3] Jennifer Mak,[3] Michael Schertzer,[3] Elizabeth A. Chavez,[3] Nancy Sawyer,[1] Peter M. Lansdorp,[3,4] Michael D. West[1]

The potential of cloning depends in part on whether the procedure can reverse cellular aging and restore somatic cells to a phenotypically youthful state. Here, we report the birth of six healthy cloned calves derived from populations of senescent donor somatic cells. Nuclear transfer extended the replicative life-span of senescent cells (zero to four population doublings remaining) to greater than 90 population doublings. Early population doubling level complementary DNA-1 (EPC-1, an age-dependent gene) expression in cells from the cloned animals was 3.5- to 5-fold higher than that in cells from age-matched (5 to 10 months old) controls. Southern blot and flow cytometric analyses indicated that the telomeres were also extended beyond those of newborn (<2 weeks old) and age-matched control animals. The ability to regenerate animals and cells may have important implications for medicine and the study of mammalian aging.

Questions have been raised as to whether cells or organisms created by nuclear transfer will undergo premature senescence. Normal somatic cells display a finite replicative capacity when cultured in vitro (*1*, *2*). The germ line appears to maintain an immortal phenotype in part through expression of the ribonucleoprotein complex telomerase, which maintains the telomeres at a long length. However, nuclear transfer technologies use embryonic, fetal, and adult somatic cells that often do not express telomerase from a range of mammalian species (*3–10*). A recent report (*11*) suggests that nuclear transfer may not restore telomeric length and that the terminal restriction fragment size observed in animals cloned from cells reflects the mortality of the transferred nucleus, which could limit the utility of the cloning of replacement cells and tissue for human transplantation (*12*, *13*).

Wilmut *et al.* (*3*) have reported that arrest in the G_0 phase of the cell cycle is required to obtain normal development of animals cloned from differentiated cells. Replicative senescence is a physiological state distinguishable from quiescence achieved by either serum starvation or density-dependent inhibition of growth of young cells (*14–18*) and appears to involve a block in late G_1 near the G_1/S boundary in the cell cycle (*19–21*), possibly reflecting a DNA checkpoint arrest (*22–26*). Here we investigate whether the production of live offspring is possible by nuclear transfer of late-passage somatic cells and whether the epigenetic changes seen in the donor cells, such as telomere shortening and loss of replicative life-span, are reflected in the resultant organism.

A somatic cell strain was derived from a 45-day-old female bovine fetus (BFF) and transfected with a PGK-driven selection cassette. Cells were selected with G418 for 10 days, and five neomycin-resistant colonies were isolated and analyzed for stable transfection by Southern blotting with a full-length cDNA probe. One cell strain (CL53) was identified as 63% (total nuclei) positive for the transgene by fluorescence in situ hybridization (FISH) analysis and was chosen for our nuclear transfer studies. These fibroblast cells, which were negative for cytokeratin and positive for vimentin, were passaged until greater than 95% of their life-span was completed, and their morphology was consistent with cells close to the end of their life-span (Fig. 1A).

A more detailed ultrastructural analysis by electron microscopy demonstrated that these cells exhibited additional features of replicative senescence, including prominent and active Golgi apparatus, increased invaginated and lobed nuclei, large lysosomal bodies, and an increase in cytoplasmic microfibrils as compared with the young cells (Fig. 1B) (*27*). In addition, these late-passage cells exhibited a senescent phenotype in showing a reduced capacity to enter S phase (Fig. 1C) and a significant increase in the staining of senescence-associated β-galactosidase (*28*, *29*). Furthermore, these cells exhibited a reduction in EPC-1 (early population doubling level cDNA-1) (*30*) mRNA levels as compared with early-passage bovine BFF cells in a manner analogous to the changes observed during the aging of WI-38 cells (Fig. 1D).

A total of 1896 bovine oocytes were reconstructed by nuclear transfer with senescent CL53 cells (*4*). Eighty-seven blastocysts (5%) were identified after a week in culture. The majority of the embryos (n = 79) were transferred into progestin (SYNCROMATE-B)-synchronized recipients (2 to 6 years old), and 17 of the 32 recipients (53%) were pregnant by ultrasound 40 days after transfer. One fetus was electively removed at week 7 of gestation (ACT99-002), whereas nine (29%) remained pregnant by 12 weeks of gestation. Two of these aborted at days 252 (twins) and 253, and one was delivered stillborn at day 278. The remaining six recipients continued development to term. The rates of blastocyst formation (5%) and early (53%) and term (19%) pregnancies with senescent CL53 cells were comparable to those of control embryos produced with nonsenescent donor (CL57) cells from early-passage cells (5, 45, and 13%, respectively).

Six calves were delivered by elective cesarean section (Fig. 2). Genomic analyses confirmed the presence of the transgene in two of the animals (CL53-1 and CL53-12), as well as in the fetus that was removed electively at day

[1]Advanced Cell Technology, One Innovation Drive, Worcester, MA 01605, USA. [2]Lankenau Institute for Medical Research, Wynnewood, PA 19096, and the Department of Pathology, Anatomy, and Cell Biology, Thomas Jefferson University, Philadelphia, PA 19104, USA. [3]Terry Fox Laboratory, British Columbia Cancer Research Center, 601 West 10 Avenue, Vancouver, BC, V5Z 1L3 Canada. [4]Department of Medicine, University of British Columbia, Vancouver, BC, V6T 2B5 Canada.

*To whom correspondence should be addressed. E-mail: rlanza@advancedcell.com